JACS
JOURNAL OF THE AMERICAN CHEMICAL SOCIETY

Article

Insights into the Mechanism of the Anodic N-N Bond Formation by Dehydrogenative Coupling

Tile Gieshoff, Anton Kehl, Dieter Schollmeyer, Kevin D. Moeller, and Siegfried R. R Waldvogel

J. Am. Chem. Soc., **Just Accepted Manuscript** • DOI: 10.1021/jacs.7b07488 • Publication Date (Web): 09 Aug 2017

ACS Publications

Journal of the American Chemical Society is published by the American Chemical Society. 1155 Sixteenth Street N.W., Washington, DC 20036

Insights into the Mechanism of the Anodic N-N Bond Formation by Dehydrogenative Coupling

Tile Gieshoff,[†,‡,⊥] Anton Kehl,[†] Dieter Schollmeyer,[†] Kevin D. Moeller,[⊥] Siegfried R. Waldvogel*[,†,‡]

[†]Institute of Organic Chemistry, Johannes Gutenberg University Mainz, 55128 Mainz, Germany

[‡]Graduate School Materials Science in Mainz, 55128 Mainz, Germany

[⊥]Department of Chemistry, Washington University in St. Louis, St. Louis, Missouri 63130, United States

ABSTRACT: The electrochemical synthesis of pyrazolidine-3,5-diones and benzoxazoles by N-N bond formation and C,O linkage respectively represents an easy access to medicinally relevant structures. Electrochemistry as key technology ensures a safe and sustainable approach. We gained insights in the mechanism of these reactions by combining cyclovoltammetric and synthetic studies. The electron transfer behavior of anilides and dianilides was studied and led to the following conclusion: The N-N bond formation involves a diradical as intermediate, whereas the benzoxazole formation is based on a cationic mechanism. Besides these studies, we developed a synthetic route to mixed dianilides as starting materials for the N-N coupling. The compatibility with valuable functionalities like triflates and mesylates for follow-up reactions as well as the comparison of different electrochemical set-ups also enhanced the applicability of this method.

Introduction

Pyrazolidin-3,5-diones and benzoxazoles are important heterocyclic motifs appearing in natural products and drugs.[1] Phenylbutazon,[2] pseudopteroxazole,[3] UK-1,[4] and ERB-041[5] represent just a few examples of the medicinally relevant compounds that possess these key ring skeletons. Because of this relevance, several methods to access such heterocyclic motifs have been reported.[6] Nevertheless, limitations regarding the sustainability and generality of these reactions are consistent with the need for the development of alternative methods. For example, the conventional synthesis of pyrazolidine-3,5-diones requires the use of highly carcinogenic *N,N'*-diarylhydrazines. This leads to the need for additional safety precautions and challenges in connection with reaction scale-up.[7] Moreover, complex substitutions patterns require additional synthetic steps following construction of the central ring skeleton.[8] For the synthesis of benzoxazoles, the principle synthetic strategies are based on condensation reactions involving 2-aminophenols or coupling reactions of anilide substrates. These approaches usually require elevated temperatures, catalysts, and result in significant reagent waste.[9]

As an alternative, we recently reported a simple route to pyrazolidin-3,5-diones via the electrochemical formation of a N-N bond. The reactions can be conducted in a simple undivided cell at constant current conditions.[10] This approach dispenses with the need of toxic *N,N'*-diarylhydrazines and gives a straightforward access to more complex substitution patterns. When the approach was applied to the formation of six-membered rings, we learned that a the slower N-N bond formation led to competitive formation of a benzoxazole ring by the generation of a C,O linkage.[11] While the yield of the reaction was low, the finding suggested that it might be possible to convert easy accessible anilides into either a pyrazolidin-3,5-dione or benzoxazoles by the control of reactions conditions and selection of substrates. However, developing such a strategy requires an understanding of the reaction mechanisms that govern product formation in two competing pathways. We report here those mechanistic details along with a general strategy for elucidating the pathways that originate from the generation of an amidyl radical intermediate under oxidative conditions.

Scheme 1. Competing formation of the N-N bond and C-O bond.

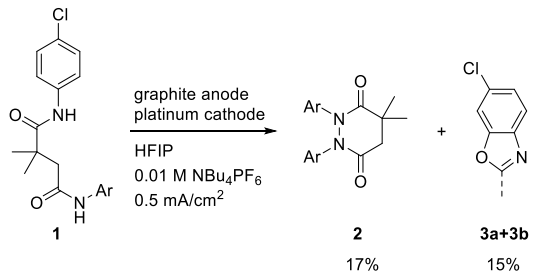

Ar = 4-chlorophenyl
HFIP = 1,1,1,3,3,3-hexafluoroisopropanol

Scheme 2. Electrochemical formation of pyrazolidin-3,5-diones and benzoxazoles.

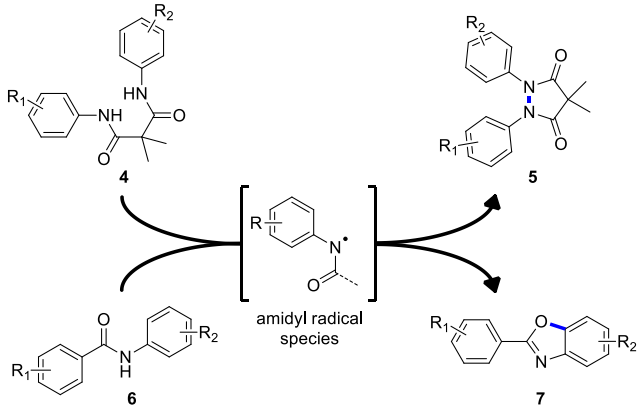

As suggested in the preceding statement, the key reactive species central to both reaction pathways is an amidyl radical. The structure, generation, and reactivity of such amidyl radicals is an important topic in contemporary research because the intermediates play a role in rearrangement reactions, cyclizations, and hydroamination reactions. The generation of amidyl radicals typically rely on the cleavage of halogenated amides.[12] In contrast, the electrochemical approach used here allows for the direct formation of the intermediates from an amide, and hence the generation of amidyl radicals from non-activated starting materials. The use of electrochemistry for the oxidation reactions was selected because of the opportunities it provides for sustainability and extraordinary reaction pathways.[13] In the current reactions, only a minimal amount of waste is generated and electric current serves as inexpensive and renewable redox reagent. The use of a low supporting electrolyte concentration (0.01 M) and 1,1,1,3,3,3-hexafluoroisopropanol (HFIP) as a recyclable solvent minimized both reagent use and the fluorine footprint of the reaction. HFIP has a key role in these transformations, since it exclusively enables efficient conversions due to its radical stabilizing properties.[14]

Work to understand the mechanism of the current reactions initially focused on the formation of N-N bonds. This effort was motivated by the synthetic potential of the reactions, and the opportunity to further enhance that potential by expanding the scope of the reactions to include substituents (like triflates[15] or mesylates[16]) that are compatible with further elaboration of the products. The key, of course, is understanding how such substituents alter the reactivity of the intermediates involved, an understanding that not only impacts the current reactions but potentially a wide variety of oxidative processes.

Results and Discussion

Elucidation of Mechanistic Assumptions. The electrochemical N-N bond formation reaction is initiated by the direct oxidation of the anilide at the anode. After a single electron transfer (SET), the radical cation formed is more acidic than the corresponding anilide by several orders of magnitude.[17] Deprotonation of the radical cation is fast and, in this case, can be supported by cathodically generated alcoholate anions derived from HFIP. After generation of the amidyl radical, there are two possible mechanistic pathways that can be followed. One possibility is that the amidyl radical will be oxidized again at the anode to form a cation (**II**). This cation is then trapped by the second anilide to form the N-N bond. The second involves an oxidation not of the amidyl radical but of the second anilide present in the substrate. In this case, the N-N bond would be formed by an intramolecular recombination of diradical **I**.

Scheme 3. General Steps of the Anilide Oxidation and Possible Mechanisms of the N-N Bond Formation to Pyrazolidine-3,5-diones.

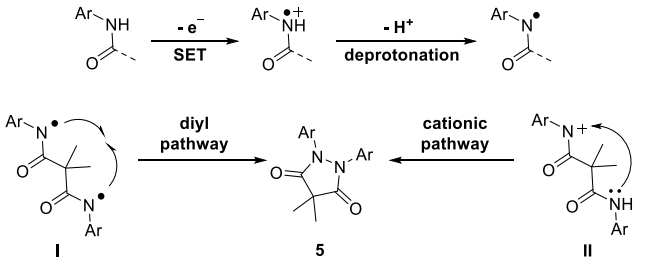

In order to differentiate these possibilities, it is important to understand the oxidation potentials involved. If the oxidation potential (E_{ox}) of the amidyl radical (Scheme 2) is lower than the oxidation potential of the other anilide site, the formation of cation **II** would be favored. If the oxidation potential of the second anilide is lower than the amidyl radical, then the formation of diradical **I** would be promoted. To gain insight into these relative oxidation potentials, we undertook an electroanalytical study to complement the synthetic investigations. It was our hope that a combination of oxidation potential measurements and synthetic verification of the insights provided would allow us to distinguish between the two possible mechanistic pathways.

Cyclovoltammetric Measurements of Test Substrates. Since it is not possible to measure the oxidation potential of an isolated anilide moiety in a dianilide, the oxidation potentials were measured for a monoanilide test substrate. Pivaloyl anilides with different substitution patterns were used to test the electronic parameters required for a successful reaction. The substrates were easily accessible by treatment of the corresponding anilines with pivaloyl chloride. Each substrate was then investigated by cyclic voltammetry in order to determine the oxidation potential for both the initial anilide ($E_{ox,1}$) and the resulting amidyl radical ($E_{ox,2}$) (Scheme 4).

Scheme 4. Oxidation steps of anilides.

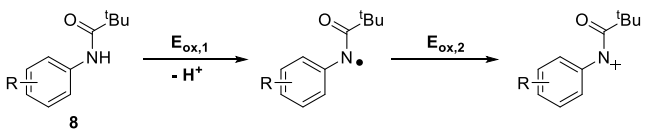

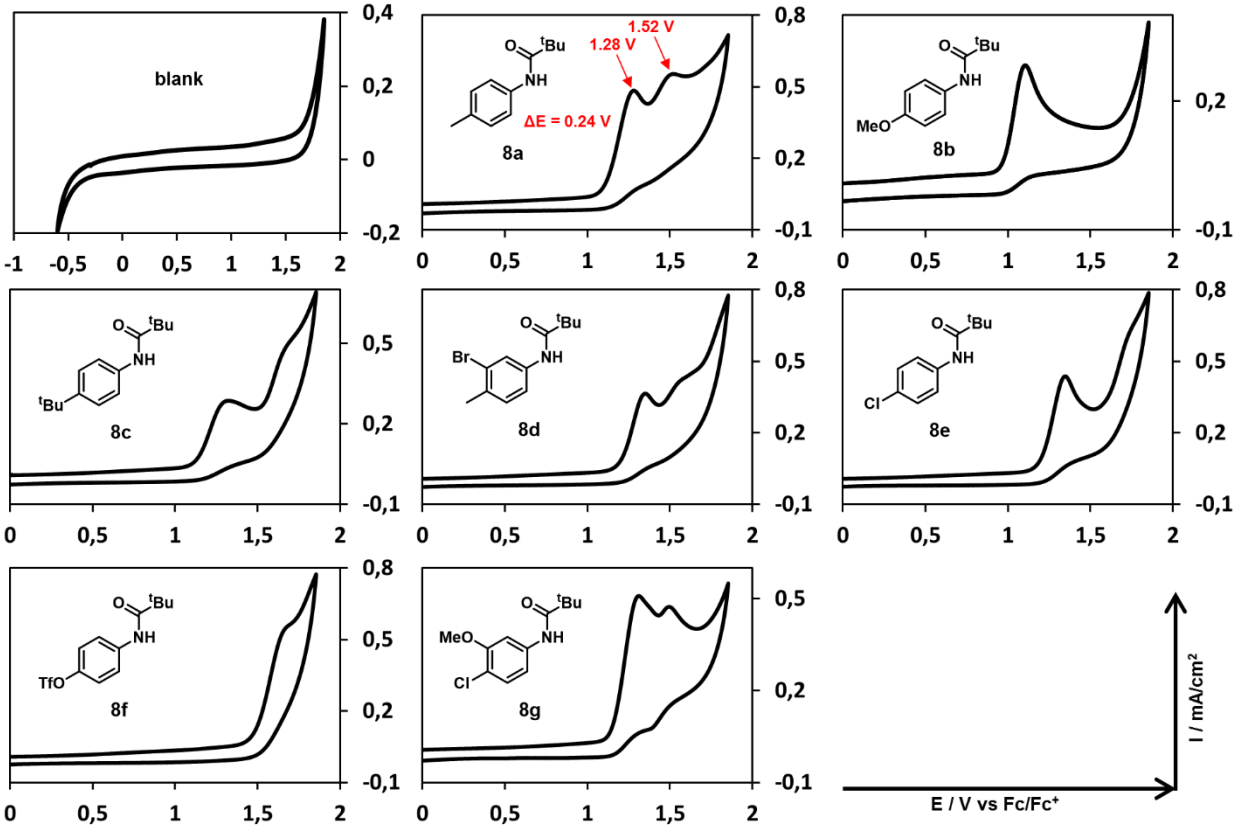

Figure 1. Cyclic voltammogramms of pivaloyl anilides as test compounds (Conditions: 1 mM substrate in 0.1 M NBu_4PF_6 (5 mL), WE: glassy carbon, CE: glassy carbon, RE: Ag/AgCl in sat. LiCl in EtOH, scan rate: 200 mV/s), final reference vs. FcH/FcH^+.

Figure 1 displays the cyclic voltammogramms of the pivaloyl derivatized anilines. The blank measurement reveals a potential limit of the electrolyte around 1.8 V and -0.5 V vs. Fc/Fc^+. In the voltammogramms of compounds **8a and 8c-8g**, two distinct oxidation peaks are visible. Depending on the substitution pattern, the $E_{ox,1}$ peak can overlap with the current at the potential limit, leading to "shoulder-shaped" peaks. This becomes most visible at substrate **8f**. Since it demands a higher voltage to oxidize the corresponding amidyl radical, the peak for the $E_{ox,2}$ step frequently shows this behavior. In the case of the triflate substituted derivative (**8f**), $E_{ox,2}$ is completely buried under the potential limit wave. The results of the cyclovoltammetric measurements are in accordance with the electron density of the aromatic ring. The voltage difference of $E_{ox,1}$ and $E_{ox,2}$ dependents on the substituents on the rings and their ability to stabilize cation formation. For example, *para*-methyl groups lead to a smaller voltage difference (**8a** 240 mV and **8d** 230 mV, respectively) than other substrates (**8c** 380 mV and **8e** 410 mV, respectively). For substrate **8b** with the even more electron-releasing *para*-methoxy group, no difference between the two oxidation potentials was observed. The second oxidation step is favored, since the cation formed is stabilized by resonance by the methoxy group as a quinone imine-like structure. Substrate **8g** results in a differently shaped voltammogramm with a low peak current of the $E_{ox,2}$ step. The small current seen for the amidyl oxidation is consistent with decomposition of the amidyl radical, a suggestion that manifests at the low yield of product obtained from reactions with this substrate (see below). A rationale might be the interplay of the electron-withdrawing chloro substituent and the strong electron-releasing methoxy-group, potentially leading to polymerization and decomposition. Table 1 displays the data for both oxidation steps.

Table 1. Oxidation potentials $E_{ox,1}$ and $E_{ox,2}$ of test substrates vs Fc/Fc^+.

Entry	Substrate	$E_{ox,1}$ / V	$E_{ox,2}$ / V
1	**8a**	1.28	1.52
2	**8b**	1.10	1.10
3	**8c**	1.31	1.69
4	**8d**	1.34	1.57
5	**8e**	1.35	1.76
6	**8f**	1.69	-
7	**8g**	1.31	1.49

This study was conducted to achieve an insight into the electron transfer steps of the electrochemical oxidation of anilides.

In general, the measurement of two distinct peaks for oxidations steps immediately suggested a diyl mechanism, since symmetric dianilides always lead to N-N bond formation.[10] With the success of these studies, attention was turned toward understanding the more complex dianilide systems.

Synthesis and Electrolysis of Mixed Dianilides. Based on oxidation potentials of the individual anilide moieties, we synthesized several mixed dianilides. We focused on the combination of anilides with E_{ox} values, which based on the data presented would lead either to the formation of a diradical or to the formation of a cation. The goal was to probe what products would form from each of the proposed mechanistic pathways. In addition, the selective access to mixed dianilides enables both the synthesis of a variety of products and the ability to design a product that is ideally functionalized for further development in subsequent synthetic transformations. In order to gain access to a variety of dianilides, the synthetic route shown in Scheme 5 was developed. In this chemistry, a coupling reaction was performed using substrate **9** and a variety of anilines, the alcohol converted to an acid, and then a second coupling performed. The oxidation step in the sequence could be conducted with a catalytic amount of the chromate reagent in a number of cases.[18]

Scheme 5. Synthetic route to mixed dianilides.

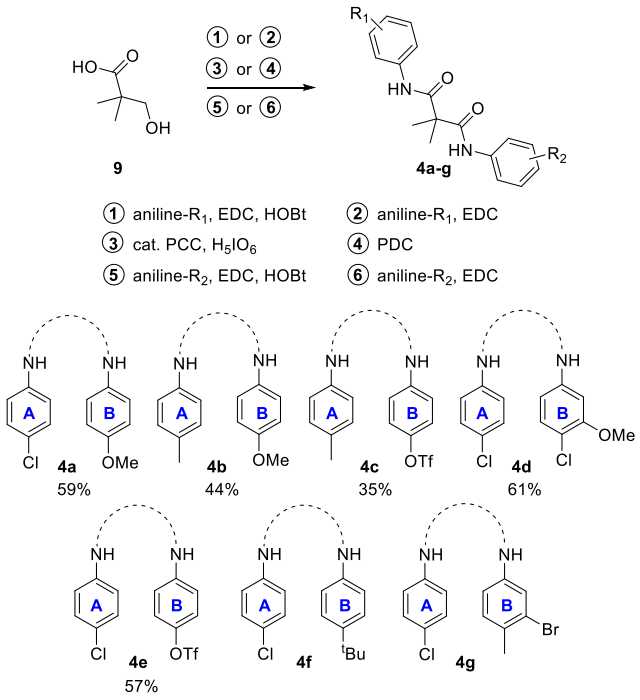

The detailed syntheses of the substrates can be found in the supporting information. One variation of note here is that the synthesis of the triflate derivatives **4c** and **4e** could not be obtained directly from the chemistry shown. In these cases, the phenol derivative was initially synthesized and the triflate group added with triflic anhydride in a subsequent step.[19]

An overview about the oxidation potentials of the combined anilide sites and the corresponding products are displayed in Table 2. The electrolysis products of the conversion are shown in Chart 1. If we take the determined E_{ox} data of the test substrates into account for the prediction of the electron transfer behavior, mixed dianilides **4a**, **4b**, and **4c** are expected to form a cationic intermediate, and substrates **4d**, **4e**, **4f**, and **4g** a diradical intermediate. For example, consider the data shown for substrate **4a**. In this case, both the oxidation potentials for anilide site B (1.10 V) are below the initial potential for site A (1.35 V). Hence, the second oxidation at site B should occur prior to the initial oxidation at site A; the conditions required for cation formation. Compare that data with that for substrate **4d**. Here, the second oxidation at site B occurs at a higher potential than the initial oxidation at site A; the conditions required for diradical behavior.

Table 2. Overview of the electrolysis of mixed dianilides.

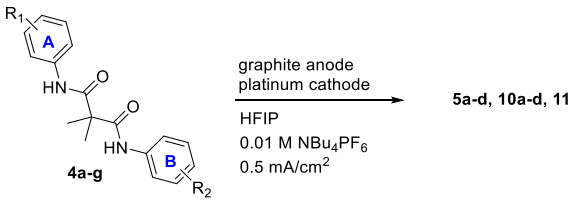

Entry	Substrate	Anilide site	$E_{ox,1}$ / V*	$E_{ox,2}$ / V*	Product
1	**4a**	**A**	1.35	1.76	**10a (56%)**
		B	1.10	1.10	
2	**4b**	**A**	1.28	1.52	**10b (60%)**
		B	1.10	1.10	
3	**4c**	**A**	1.28	1.52	**10c (37%)**
		B	1.69	-	
4	**4d**	**A**	1.35	1.76	**11 (10%) 5a (11%)**
		B	1.31	1.49	
5	**4e**	**A**	1.35	1.76	**5b (34%)**
		B	1.69	-	
6	**4f**	**A**	1.35	1.76	**5c (49%)**
		B	1.31	1.69	
7	**4g**	**A**	1.35	1.76	**5d (55%)**
		B	1.34	1.57	

*Red color indicates that these are the first two proceeding oxidation steps.

Chart 1. Electrolysis products derived from the conversion of mixed dianilides.

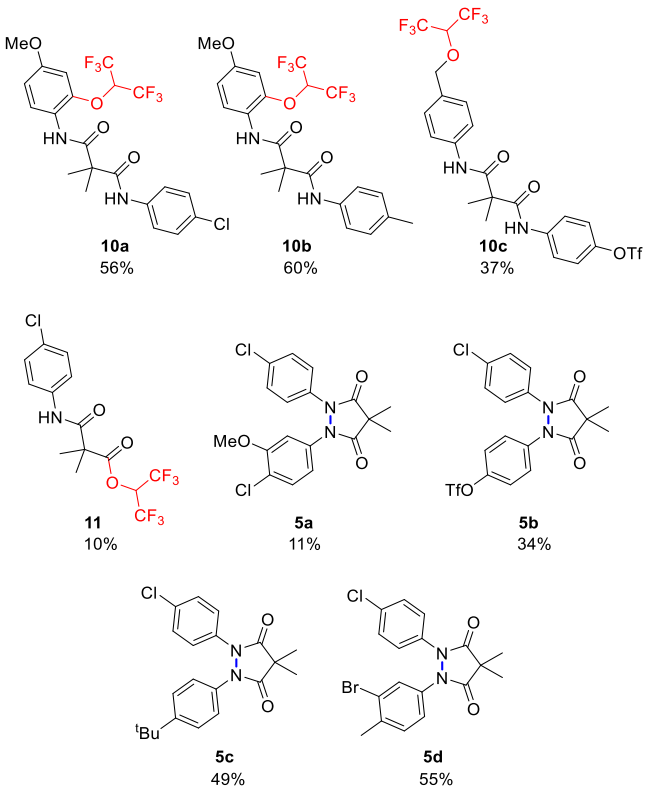

[a]Yields for substrate **5c** and **5d** were already reported in a former publication.

The electrolysis of the mixed dianilides revealed the formation of interesting products. Instead of forming the N-N bond, dianilides **4a**, **4b**, and **4c** formed HFIP incorporated products **10a**, **10b**, and **10c** and only small traces of N-N bond formed products were detectable. When *para*-methoxy substituted anilides were used, the addition of HFIP occurred at the aromatic *ortho*-position. In case of a *para*-methyl substitution, addition occurred at the benzylic position. This substitution is most consistent with the loss of a proton from the cationic intermediate (**IV**) to form an azoquinone methide derivative. This result would appear to confirm the accuracy of the prediction made based on the oxidation potentials shown in Table 2. Compounds **4e**, **4f**, and **4g** formed pyrazolidine-3,5-diones **5b**, **5c**, and **5d** as products by an N-N bond formation. The E_{ox} values for these compounds were all consistent with the formation of a diradical intermediate. Substrate **4d** formed a product (**10d**) consistent with alcoholysis of the amidyl group along with the desired pyrazolidine-3,5-dione product (**5a**). This decomposition product is consistent with the different CV behavior for the group noted above in connection with Figure 1. Based solely on the oxidation potentials, N-N bond formation is more likely than cation formation, so at this time the mechanistic origin of the decomposition pathway remains unsolved. Competing diradical and cationic pathways are possible.

Cyclovoltammetric Measurements of Mixed Dianilides. Beside the cyclovoltammetric study of the test substrates and the synthetic study, we were also interested in the electron transfer behavior of the dianilides within a cyclic voltammetric study.

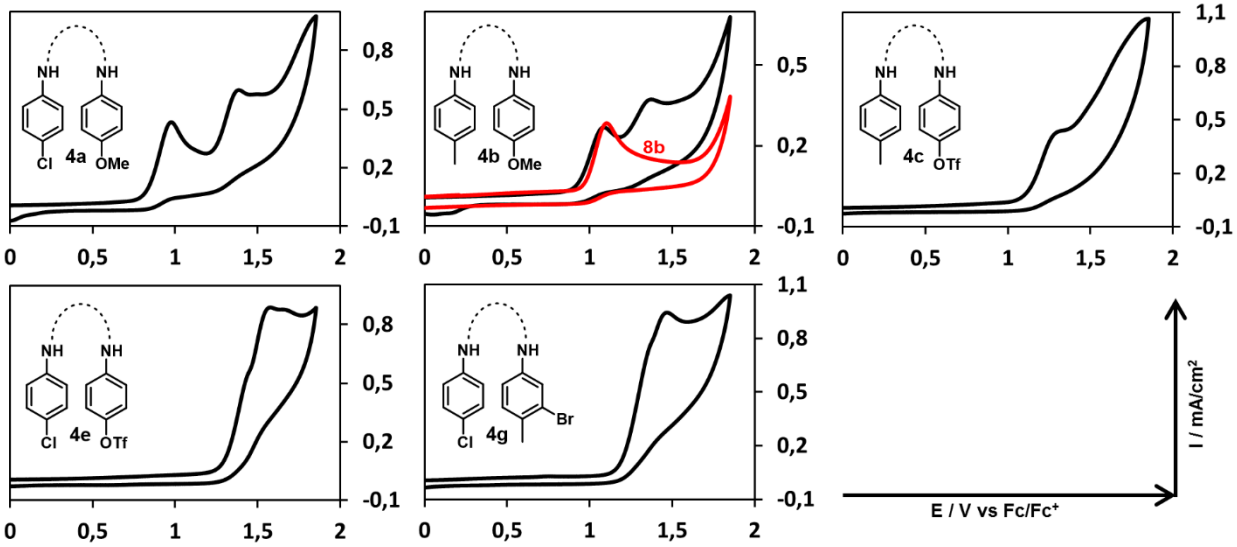

Figure 2. Cyclic voltammogramm of mixed dianilides (Conditions: 1 mM substrate in 0.1 M NBu_4PF_6 (5 mL), WE: glassy carbon, CE: glassy carbon, RE: Ag/AgCl in sat. LiCl in EtOH, scan rate: 200 mV/s), final reference vs. FcH/FcH^+.

As expected, the voltammogramms of the mixed dianilides demonstrate a different electron transfer behavior for cation forming and diradical forming dianilides. The voltammogramms substrates **4a**, **4b**, and **4c** show a significant difference between the oxidation potentials of the two groups, whereas compounds **4e** and **4g** reveal two oxidation peaks very close to each other. This data once again suggests cation formation in **4a**-c and diradical formation for substrates **4e** and **4g**. In this way, the data is again fully consistent with the observations made above. It appears

that N-N bond formation is the result of a diradical intermediate (Scheme 3, intermediate **I**).

Theoretical considerations also support this argument. The unpaired electron can populate both, σ- and π-orbitals, while the exact structure depends on many factors, e.g. substitution pattern.[20] Moreover, there is an attractive interaction among σ–radical and σ*–orbital. The corresponding cation is located in the π-orbital and stabilized by the aromatic ring. It is likely that a σ-radical facilitates the subsequent recombination, whereas a π-cation would exacerbates a selective cyclization reaction and rather leads to side reactions.

Adaption to the Benzoxazole Mechanism. As mentioned in the introduction, much of this work was motivated by the opportunity to generate both the N-N bond forming products and benzoxazole products from closely related substrates. The benzoxazole was initially a unexpected side product found in a reaction planned for N-N bond formation. With an understanding of how the N-N bond forming reactions can be designed, we were in position to tackle the challenge of selectively generating the benzoxazole ring system. One observation made during the synthesis of benzoxazoles[11] provided significant guidance for this endeavor. That observation is that a *para*-methyl substitution on the anilide significantly inhibits benzoxazole formation. Instead, the reactions tend to lead to HFIP ether derivatives (**6a**) in a fashion directly analogous to the earlier formation of product **10c**. This finding was initially unexpected, since *para*-methyl groups are beneficial for the generation of N-N bonds. This suggested that benzoxazole formation might be derived from the generation of a cationic intermediates. In such a case, the formation of amidyl cation (**III**) can lead to deprotonation at the benzylic carbon, the formation of an azoquinone methide (**IV**), and solvent trapping. The combination of this finding with the mechanistic study above led us to conclude that the mechanism for the benzoxazole formation most likely proceeds through a cationic intermediate (**III**), which can undergo an oxa-Nazarov-type cyclization.[21]

Scheme 6. Solvent trapping product and the cationic intermediate in the benzoxazole formation.

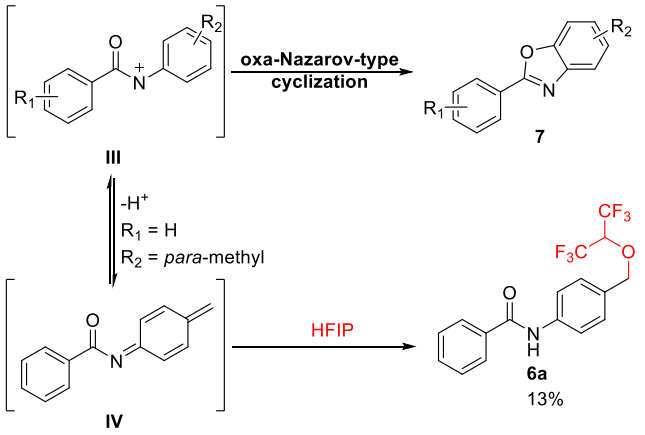

With this knowledge, the design of new substrates for benzoxazole products becomes viable. In this context, it is interesting to note that in the benzoxazole syntheses, the solvent trapping products that appear to interfere with the N-N bond forming reactions above are not a problem, even when *para*-methoxy groups are present (Chart 1). This divergent behavior originates from a competition between carbonyl oxygen addition to the aryl ring (benzoxazole formation) and solvent (HFIP) trapping of the ring. This competition is shifted toward solvent trapping when a dianilide is used as the substrate. It appears that hydrogen bonding between the carbonyl and the second anilide in the molecule lowers the nucleophilicity of the carbonyl oxygen and favors HFIP addition. The hydrogen bonding is detectable in crystallographic studies of substrate **10c** (see supporting information).

Optimization of scope and reaction set-up. With the mechanism for the reaction determined, we turned our attention toward evaluating the synthetic scope and utility of the reactions. In our previous work, *para*-chloro and *meta*-bromo substitutions were most valuable from a synthetic point of view. However, the latter only afforded the desired N-N product in a 33% yield. Moreover, the reactions were restricted to products that contained a para-substituent.[10] With the selective synthesis for mixed dianilides and the mechanistic insights in hand, these limitations could be addressed. To this end, the chemistry was explored for its compatibility with synthetically versatile triflate and mesylate groups. In addition, we investigated the influence of bulky *meta*-substitutions in order to determine if they would prevent side reactions at substituent-free *para*-positions. As shown in Chart 2, the conversion of symmetric triflates and mesylates substrates into the desired products showed that the groups were tolerated by the reactions, and the use of a bulky *meta*-substituent did have a positive effect on the reactions.

Chart 2. Extension of the scope to triflates, mesylates, and *para*-unblocked derivatives.[a]

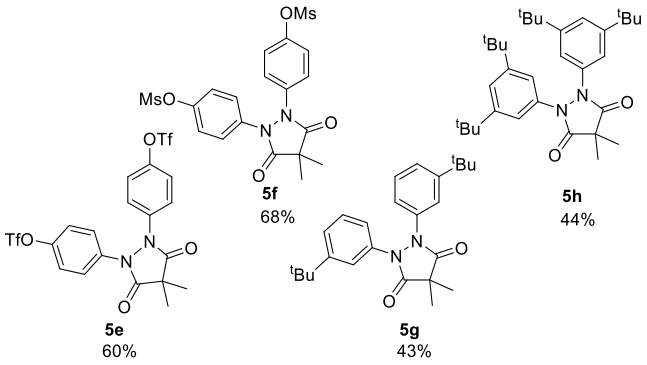

The formation of **5b** was particularly interesting because it involved the generation of an unsymmetrical product wherein the two aromatic rings were synthetically differentiated, but the initial yield for this reaction was low (34%). When we worked on the benzoxazoles formation, we demonstrated the utility of varying the reaction setup as a means of optimizing the yield for a particular product.[11] With several substrates, we tested the two main electrochemical setups used for constant current electrolysis with regards to their influence on the N-N bond formation. Set-up **A** includes a beaker-type cell with a flat isostatic graphite anode and a platinum plate cathode in a parallel orientation to each other.[22] Set-up **B** is based on a 25 mL three-necked flask with a reticulated vitreous carbon (RVC) anode and a platinum wire cathode placed angularly to each other. Chart 3 demonstrates that the performance of the cells was dependent on the the substrate used. On one hand, compound **5b** was isolated in 84%, when set-up **B** was used. On the other hand, set-up **A** worked better with compound **5j**. Compound **5i** gives similar yields in both set-ups, but RVC as anode material enables higher currents and therefore a more time-efficient conversion. It is important to note that for an initial pass, either setup can be used to test the viability of a reaction. One can then adjust the nature of the reaction setup after it is clear that the electrolysis works.

Chart 3. Comparison of electrolysis set-up.[a]

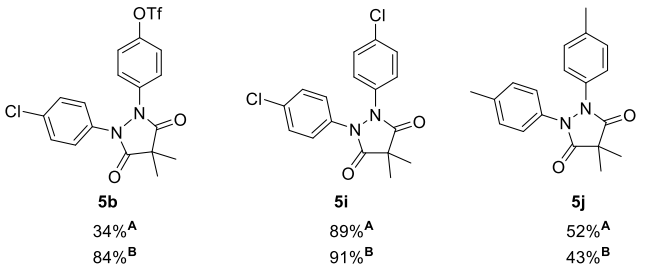

[a]Yield for substrate **11e** and **11f** using set-up **A** were already reported in a previous publication, isolated from a 25 mL cell.[10]

Figure 3. Set-ups **A** (left) and **B** (right).

Conclusion

The advancement of electroorganic synthesis is dependent on both, the development of new reactions of synthetic value and the development of the mechanistic insights necessary to make conclusions about and extend the scope of those reactions. In the example presented here, we outlined both, the synthetic potential of anodic oxidations leading to amidyl radicals and subsequent N-N bond formation reaction and benzoxazole synthesis and data supporting the mechanistic parameters that govern product formation. In addition, we highlighted how a combination of cyclovoltammetric and synthetic studies can be used to gain those insights. N-N bond formation in the systems studied is the result of a diradical coupling mechansim, whereas benzoxazole formation is the result of a cationic oxa-Nazarov-type cyclization. These insights led to the formation of products from mixed dianilide substrates, the use of synthetically valuable triflate and mesylate substrates in the reactions, and an important illustration of how different reaction set-ups can be used to optimize an electro-organic conversion.

Experimental Section

Electrolysis Protocol, Set-up A. A solution of 0.2 mmol electrolysis substrate and 19 mg tetrabutylammonium hexafluorophosphate (0.01 M) in 5 mL hexafluoroisopropanol (HFIP) is placed in a 5 mL Teflon cell.[22] The solution is electrolyzed with a current of 0.5 mA/cm^2 (active electrode area 1.6 cm^2) using an isostatic graphite plate anode and a platinum plate cathode, until 2-3 F are applied. The conversion is controlled via GC. After electrolysis, the solvent is recovered by distillation and the product is isolated via column chromatography on silica with mixtures of cyclohexane and ethyl acetate.

Electrolysis Protocol, Set-up B. A solution of 0.4 mmol anilide derivative and 38 mg tetrabutylammonium hexafluorophosphate (0.01 M) in 10 mL hexafluoroisopropanol (HFIP) is placed in a 25 mL three-necked round-bottom flask. A reticulated vitreous carbon (100 PPI) anode and a platinum wire cathode is placed in the solution and sonicated for 30 s. The solution is electrolyzed with a constant current of 8.4 mA until 2-2.2 F are applied. Full conversion is checked by TLC. After electrolysis, the solvent is removed via distillation and product is isolated

via column chromatography on silica with mixtures of hexanes and ethyl acetate.

Cyclic Voltammetry Protocol. A 1 mM solution of substrate in 5 mL HFIP (0.1 M $TABPF_6$) was placed in a 10 mL cell. Cyclic voltammetry was performed with a 200 mV/s scan rate using a glassy carbon working electrode, glassy carbon counter electrode, and Ag/AgCl reference electrode in saturated LiCl in EtOH. The peak potentials were referenced versus Fc/Fc^+ and in case of an overlap, the exact value was determined by calculating the minimum of the slope.

Synthesis and Characterization of Electrolysis Products. *N*-(4-chlorophenyl)-*N*'-(2-(1,1,1,3,3,3-hexafluoropropan-2-yloxy)-4-methoxy)-2,2-dimethylmalondiamide (**10a**). Electrolysis in set-up **A** yielded 57 mg colorless oil (0.11 mmol, 56%): ^{1}H NMR (400 MHz, $CDCl_3$) δ = 9.20 (s, 1H), 8.36 (s, 1H), 8.21 (d, *J* = 9.0 Hz, 1H), 7.63 – 7.48 (m, 2H), 7.38 – 7.24 (m, 2H), 6.72 (dd, *J* = 9.0, 2.6 Hz, 1H), 6.61 (d, *J* = 2.6 Hz, 1H), 4.91 (hept, J = 5.6 Hz, 1H), 3.83 (s, 3H), 1.68 (s, 6H); ^{13}C NMR (101 MHz, $CDCl_3$) δ = 172.58, 170.26, 157.26, 147.89, 136.43, 129.22, 128.91, 123.30, 121.35, 121.16, 120.78 (q, *J* = 280.9 Hz), 108.57, 101.97, 76.53 (hept, *J* = 33.7 Hz), 55.75, 50.89, 24.03; ^{19}F NMR (377 MHz, $CDCl_3$) δ = -74.64; HRMS for $C_{21}H_{19}{}^{35}ClF_6N_2O_4$ (ESI+) $[M+Na]^+$: calc.: 535.0835, found: 535.0845.

N-(2-(1,1,1,3,3,3-hexafluoropropan-2-yloxy)-4-methoxy)-*N*'-(4-methylphenyl)-2,2-dimethylmalondiamide (**10b**). Electrolysis in set-up **A** yielded 58 mg colorless oil (0.12 mmol, 58%): ^{1}H NMR (400 MHz, $CDCl_3$) δ = 8.88 (s, 1H), 8.22 (s, 1H), 8.22 (d, *J* = 9.0 Hz, 1H), 7.54 – 7.39 (m, 2H), 7.21 – 7.08 (m, 2H), 6.71 (dd, *J* = 9.0, 2.5 Hz, 1H), 6.61 (d, *J* = 2.3 Hz, 1H), 4.94 (hept, J = 5.5 Hz, 1H), 3.81 (s, 3H), 2.32 (s, 3H), 1.68 (s, 6H); ^{13}C NMR (101 MHz, $CDCl_3$) δ = 172.45, 170.29, 157.10, 147.90, 135.21, 133.99, 129.39, 123.29, 121.65 (q, *J* = 280.9 Hz), 121.56, 120.01, 108.49, 101.96, 76.22 (hept, *J* = 33.8 Hz), 55.70, 50.87, 23.99, 20.83; ^{19}F NMR (377 MHz, $CDCl_3$) δ = -74.63; HRMS for $C_{22}H_{22}F_6N_2O_4$ (ESI+) $[M+Na]^+$: calc.: 515.1381, found: 515.1390.

N-(4-(1-(1,1,1,3,3,3-hexafluoropropan-2-yloxy)-methyl)phenyl)-*N*'-(4-trifluoromethylsulfonyloxyphenyl)-2,2-dimethylmalondiamide (**10c**). Electrolysis in set-up **A** yielded 45 mg colorless solid (0.07 mmol, 37%): mp 102.0-103.0 °C (cyclohexane); ^{1}H NMR (400 MHz, $CDCl_3$) δ = 8.90 (s, 1H), 8.33 (s, 1H), 7.67 – 7.61 (m, 2H), 7.59 – 7.52 (m, 2H), 7.36 – 7.30 (m, 2H), 7.25 – 7.19 (m, 2H), 4.82 (s, 2H), 4.10 (hept, J = 5.9 Hz, 1H), 1.68 (s, 6H ^{13}C NMR (101 MHz, $CDCl_3$) δ = 171.90, 171.29, 145.57, 137.69, 137.53, 131.35, 129.60, 121.97, 121.54, 121.51 (q, *J* = 284.5 Hz), 120.65, 118.71 (q, J = 320.5), 75.37, 74.26 (hept, *J* = 33.3 Hz), 50.91, 24.12; ^{19}F NMR (377 MHz, $CDCl_3$) δ = -73.95, -74.74; HRMS for $C_{22}H_{19}F_9N_2O_6$ (ESI+) $[M+H]^+$: calc.: 611.0898, found: 611.0916.

N-(4-chlorophenyl)-*O*-(1,1,1,3,3,3-hexafluoropropan-2-yl)-2,2-dimethylmalonmonoamide (**11**). Electrolysis in set-up **A** yielded 8 mg colorless oil (0.020 mmol, 10%): ^{1}H NMR (400 MHz, $CDCl_3$) δ = 7.86 (s, 1H), 7.49 – 7.42 (m, 2H), 7.38 – 7.31 (m, 2H), 5.83 (hept, J = 6.0 Hz, 1H), 1.68 (s, 6H ^{13}C NMR (101 MHz, $CDCl_3$) δ = 171.75, 167.77, 135.62, 130.12, 129.13, 121.60, 120.16 (q, *J* = 282.6 Hz), 67.25 (hept, *J* = 35.2 Hz), 50.84, 23.30; ^{19}F NMR (377 MHz, $CDCl_3$) δ = -74.32; HRMS for $C_{14}H_{12}{}^{35}ClF_6NO_3$ (ESI+) $[M+H]^+$: calc.: 392.0483, found: 392.0484.

1-(4-chlorophenyl)-2-(3-methoxy-4-chlorophenyl)-4,4-dimethylpyrazolidin-3,5-dione (**5a**). Electrolysis in set-up **A** yielded 8 mg colorless oil (0.021 mmol, 11%): ^{1}H NMR (400 MHz, $CDCl_3$) δ = 7.37 – 7.32 (m, 2H), 7.32 – 7.27 (m, 3H), 7.00 (d, *J* = 2.4 Hz, 1H), 6.79 (dd, *J* = 8.5, 2.4 Hz, 1H), 3.86 (s, 3H), 1.53 (s, 6H); ^{13}C NMR (101 MHz, $CDCl_3$) δ = 174.12,174.09, 155.31, 135.29, 134.54, 132.49, 130.28, 129.35, 123.20, 120.71, 114.18, 106.63, 56.27, 44.39, 21.81; HRMS for $C_{18}H_{16}{}^{35}Cl_2N_2O_3$ (ESI+) $[M+H]^+$: calc.: 379.0611, found: 379.0612.

1-(4-chlorophenyl)-2-(4-trifluoromethylsulfonyloxyphenyl)-4,4-dimethylpyrazolidin-3,5-dione (**5b**). Electrolysis in set-up **B** yielded 146 mg colorless solid (0.34 mmol, 84%): mp 89.0-89.5 °C (EtOAc); ^{1}H NMR (400 MHz, $CDCl_3$) δ = 7.47 – 7.41 (m, 2H), 7.38 – 7.32 (m, 2H), 7.31 – 7.25 (m, 4H), 1.52 (s, 6H); ^{13}C NMR (101 MHz, $CDCl_3$) δ = 174.24,174.04, 147.05, 135.68, 134.46, 132.65, 129.47, 123.12, 123.07, 122.19, 44.30, 21.82; ^{19}F NMR (377 MHz, $CDCl_3$) δ = -73.95; HRMS for $C_{18}H_{14}{}^{35}ClF_3N_2O_5S$ (ESI+) $[M+Na]^+$: calc.: 485.0162, found: 485.0158.

1,2-bis-(4-trifluoromethylsulfonyloxyphenyl)-4,4-dimethylpyrazolidin-3,5-dione (**5e**). Electrolysis in set-up **B** yielded 137 mg colorless solid (0.24 mmol, 60%): mp 90.4-91.4 °C (EtOAc); ^{1}H NMR (400 MHz, $CDCl_3$) δ = 7.48 – 7.41 (m, 4H), 7.33 – 7.27 (m, 4H),), 1.54 (s, 6H); ^{13}C NMR (101 MHz, $CDCl_3$) δ = 174.11, 147.18, 135.74, 122.99, 122.36, 118.63 (q, *J* = 320.8 Hz), 44.30, 21.85; ^{19}F NMR (377 MHz, $CDCl_3$) δ = -73.94; Anal. Calcd for $C_{19}H_{14}F_6N_2O_8$: C, 39.59; H, 2.45; N, 4.86; S, 11.12. Found: C, 39.74; H, 2.69; N, 4.83; S, 11.14.

1,2-bis-(4-mesylphenyl)-4,4-dimethylpyrazolidin-3,5-dione (**5f**). Electrolysis in set-up **B** with 0.31 mmol dianilide in 8 mL HFIP (30 mg NBu_4PF_6) yielded 99 mg colorless solid (0.21 mmol, 68%): mp 140.0-141.0 °C (EtOAc); ^{1}H NMR (400 MHz, $CDCl_3$) δ = 7.44 – 7.38 (m, 4H), 7.33 – 7.27 (m, 4H), 1.52 (s, 6H); ^{13}C NMR (101 MHz, $CDCl_3$) δ = 174.28, 147.08, 134.92, 123.26, 122.91, 44.27, 37.57, 21.82; HRMS for $C_{19}H_{20}N_2O_5S_2$ (ESI+) $[M+Na]^+$: calc.: 491.0559, found: 491.0566.

1,2-bis-(3-(1,1-dimethylethyl)phenyl)-4,4-dimethylpyrazolidin-3,5-dione (**5g**). Electrolysis in set-up **A** yielded 34 mg colorless oil (0.087 mmol, 43%): ^{1}H NMR (400 MHz, $CDCl_3$) δ = 7.30 – 7.24 (m, 2H), 7.23 – 7.17 (m, 6H), 1.56 (s, 6H), 1.19 (s, 18H); ^{13}C NMR (101 MHz, $CDCl_3$) δ = 173.12, 152.09, 135.25, 128.57, 123.56, 120.06, 44.54, 34.70, 31.06, 21.81; HRMS for $C_{25}H_{32}N_2O_2$ (ESI+) $[M+Na]^+$: calc.: 415.2361, found: 415.2366.

1,2-bis-(3,5-di(1,1-dimethylethyl)phenyl)-4,4-dimethylpyrazolidin-3,5-dione (**5h**). Electrolysis in set-up **A** yielded 44 mg colorless oil (0.088 mmol, 44%): ^{1}H NMR (400 MHz, $CDCl_3$) δ = 7.15 (t, *J* = 1.7 Hz, 2H), 7.03 (d, *J* = 1.7 Hz, 4H), 1.55 (s, 6H), 1.16 (s, 36H); ^{13}C NMR (101 MHz, $CDCl_3$) δ = 173.00, 151.47, 134.30, 120.23, 117.69, 44.72, 34.84, 31.18, 21.79; HRMS for $C_{33}H_{48}N_2O_2$ (ESI+) $[M+H]^+$: calc.: 505.3794, found: 505.3787.

1,2-bis-(4-chlorophenyl)-4,4-dimethyl-tetrahydropyridazine-3,6-dione (**2**). Electrolysis in set-up **A** using 1 mmol dianilide in a 25 mL cell (25 mL HFIP, 100 mg NBu_4PF_6) yielded 63 mg yellow solid (0.17 mmol, 17%): mp 211.0-211.8 °C; ^{1}H NMR (400 MHz, DMSO-d_6) δ = 7.52 – 7.46 (m, 2H), 7.44 – 7.40 (m, 2H), 7.39 – 7.34 (m, 4H) 2.93 (s, 2H), 1.24 (s, 6H); ^{13}C NMR (101 MHz, $CDCl_3$) δ = 173.22, 167.58, 136.33, 135.79, 132.49, 132.41, 129.10, 128.98, 125.58, 125.07, 43.38, 38.12, 23.49; HRMS for $C_{18}H_{16}{}^{35}Cl_2N_2O_2$ (ESI+) $[M+H]^+$: calc.: 363.0667, found: 363.0666.6-Chloro-2-(*N*-(4-chlorophenyl)-1,1-dimethyl)propanamide-1,3-benzoxazole (**3a**) and 6-Chloro-2-(*N*-(4-chlorophenyl)-2,2-dimethyl)propanamide-1,3-benzoxazole (**3b**). Electrolysis in set-up **A** using 1 mmol dianilide in a 25 mL cell (25 mL HFIP, 100 mg NBu_4PF_6) yielded 55 mg red solid as a 3:1 mixture of both isomers, whereby **3a** is the main compound (0.15 mmol, 15%): ^{1}H NMR (400 MHz, $CDCl_3$) δ = 9.14 (s, 1H), 8.81 (s, 0.2H), 7.80 (s, 0.2H), 7.65 – 7.63 (m, 1H), 7.54 (d, *J* = 1.9 Hz, 0.7H), 7.40 – 7.37 (m, 2H), 7.35 (dd, *J* = 8.5, 1.9 Hz, 0.8H), 7.23 – 7.19 (m, 2H), 2.94 (s, 1.5H), 2.93 (s, 0.5H), 1.57 (s, 6H); ^{13}C NMR (101 MHz, $CDCl_3$) δ = 174.10, 172.91, 168.38, 168.15, 150.89, 149.31, 139.98, 138.90, 136.56, 136.40, 130.86, 128.88, 125.29, 120.68, 120.62, 120.49, 119.87, 112.54, 111.45, 48.33, 48.15, 37.15, 27.09, 27.00; HRMS for $C_{18}H_{16}{}^{35}Cl_2N_2O_2$ (ESI+) $[M+H]^+$: calc.: 363.0667, found: 363.0652.

N-(4-(1-(1,1,1,3,3,3-hexafluoropropan-2-yloxy)-methyl)phenyl)benzamide (**6a**). Electrolysis in set-up **A** yielded 10 mg white solid (0.026 mmol, 13%): mp 150.0-150.3 °C ^{1}H NMR (400 MHz, $CDCl_3$) δ = 7.90 (s, 1H), 7.89 – 7.85 (m, 2H), 7.72 – 7.67 (m, 2H), 7.60 – 7.54 (m, 1H), 7.52 – 7.47 (m, 2H), 7.40 – 7.35 (m, 2H) 4.85 (s, 2H), 4.12 (hept, *J* = 6.0 Hz, 1H); ^{13}C NMR (101 MHz, $CDCl_3$) δ = 165.75, 138.63, 134.70, 132.04, 130.55, 129.76, 128.85, 127.00, 121.57 (q, *J* = 284.5 Hz), 120.22, 75.43, 74.05 (hept, *J* = 32.7 Hz); HRMS for $C_{17}H_{13}F_6NO_2$ (ESI+) $[M+H]^+$: calc.: 378.0923, found: 378.0914.

ASSOCIATED CONTENT

General information
Experimental and analytical details for the synthesis of test substrates, symmetric dianilides, and mixed dianilides, NMR spectra and crystallographic details (PDF)
Crystallographic data for **2** (CIF)
Crystallographic data for **3a** (CIF)
Crystallographic data for **10c** (CIF)
This material is available free of charge via the Internet at http://pubs.acs.org."

AUTHOR INFORMATION

Corresponding Author

*waldvogel@uni-mainz.de

Author Contributions

All authors have given approval to the final version of the manuscript.

ACKNOWLEDGMENT

T. G. is a recipient of a DFG fellowship by the Excellence Initiative by the Graduate School Materials Science in Mainz (GSC 266). The work done in the labs of KDM was supported by the US National Science Foundation (CHE-1463913). The support by The Advanced Lab for Electrochemistry and Electrosynthesis – ELYSION (Carl Zeiss Stiftung) and the DFG (WA 1276/17-1) is highly appreciated.

ABBREVIATIONS

WE working electrode; RE reference electrode; CE counter electrode; FcH Ferrocene.

REFERENCES

(1) a) Aiba née Kaneko, M.; Hirota, M.; Kouzuki, H.; Mori, M. *J. Toxicol. Sci.* **2015**, *40*, 77–98; b) Zhang, X.-Y.; Gu, Y.-F.; Chen, T.; Yang, D.-X.; Wang, X.-X.; Jiang, B.-L.; Shao, K.-P.; Zhao, W.; Wang, C.; Wang, J.-W.; Zhang, Q.-R.; Liu, H.-M. *Med. Chem. Commun.* **2015**, *6*, 1781–1786; c) Nishiu, J.; Ito, M.; Ishida, Y.; Kakutani, M.; Shibata, T.; Matsushita, M.; Shindo, M. *Diabetes, Obes. & Metab.* **2006**, *8*, 508–516; d) Deng, G.; Li, W.; Shen, J.; Jiang, H.; Chen, K.; Liu, H. *Bioorg. Med. Chem. Lett.* **2008**, *18*, 5497–5502; e) Gilbert, A. M.; Failli, A.; Shumsky, J.; Yang, Y.; Severin, A.; Singh, G.; Hu, W.; Keeney, D.; Petersen, P. J.; Katz, A. H. *J. Med. Chem.* **2006**, *49*, 6027–6036; f) Kutterer, K. M.; Davis, J. M.; Singh, G.; Yang, Y.; Hu, W.; Severin, A.; Rasmussen, B. A.; Krishnamurthy, G.; Failli, A.; Katz, A. H. *Bioorg. Med. Chem. Lett.* **2005**, *15*, 2527–2531;

(2) Steinhilber, D.; Schubert-Zsilavecz, M.; Roth, H. J. *Medizinische Chemie: Targets, Arzneistoffe, Chemische Biologie*; Dt. Apotheker-Verlag: Stuttgart, 2010.

(3) Davidson, J. P.; Corey, E. J. *J. Am. Chem. Soc.* **2003**, *125*, 13486–13489.

(4) M. Ueki; K. Ueno; S. Miyadoh; K. Abe; K. Shibata; M. Taniguchi; S. Oi. *J. Antibiot.* **1993**, *46*, 1095–1100.

(5) Leventhal, L.; Brandt, M. R.; Cummons, T. A.; Piesla, M. J.; Rogers, K. E.; Harris, H. A. *Eur. J. Pharmacol.* **2006**, *553*, 146–148.

(6) a) Alvarez-Builla, J.; Vaquero, J. J.; Barluenga, J. *Modern Heterocyclic Chemistry*; Wiley-VCH Verlag GmbH & Co. KGaA: Weinheim, Germany, 2011; b) Joule, J. A.; Mills, K. *Heterocyclic Chemistry*, 5. Aufl.; Wiley-Blackwell: s.l., 2013; c) Francke, R. *Beilstein J. Org. Chem.* **2014**, *10*, 2858–2873;

(7) a) *Carcinog. Tech. Rep. Ser. - U. S., Natl. Cancer Inst.* **1978**, *92*, 1–123; b) Dodd, D. E.; Pluta, L. J.; Sochaski, M. A.; Wall, H. G.; Thomas, R. S. *Int. J. Toxicol.* **2013**, *31*, 564–571;

(8) Li, G.-Q.; Gao, H.; Keene, C.; Devonas, M.; Ess, D. H.; Kürti, L. *J. Am. Chem. Soc.* **2013**, *135*, 7414–7417.

(9) a) Mayo, M. S.; Yu, X.; Zhou, X.; Feng, X.; Yamamoto, Y.; Bao, M. *J. Org. Chem.* **2014**, *79*, 6310–6314; b) Ueda, S.; Nagasawa, H. *J. Org. Chem.* **2009**, *74*, 4272–4277; c) Khatun, N.; Guin, S.; Rout, S. K.; Patel, B. K. *RSC Adv.* **2014**, *4*, 10770; d) Alla, S. K.; Sadhu, P.; Punniyamurthy, T. *J. Org. Chem.* **2014**, *79*, 7502–7511;

(10) Gieshoff, T.; Schollmeyer, D.; Waldvogel, S. R. *Angew. Chem. Int. Ed.* **2016**, 55, 9437–9440.

(11) Gieshoff, T.; Kehl, A.; Schollmeyer, D.; Moeller, K. D.; Waldvogel, S. R. *Chem. Commun.* **2017**, 53, 2974–2977.

(12) Zard, S. Z. *Chem. Soc. Rev.* **2008**, *37*, 1603.

(13) a) Horn, E. J.; Rosen, B. R.; Baran, P. S. *ACS Cent. Sci.* **2016**, *2*, 302–308; b) Frontana-Uribe, B. A.; Little, R. D.; Ibanez, J. G.; Palma, A.; Vasquez-Medrano, R. *Green Chem.* **2010**, *12*, 2099–2119; c) Yoshida, J.-i.; Kataoka, K.; Horcajada, R.; Nagaki, A. *Chem. Rev.* **2008**, *108*, 2265–2299; d) Waldvogel, S. R.; Möhle, S. *Angew. Chem. Int. Ed.* **2015**, *54*, 6398–6399; e) Waldvogel, S. R.; Janza, B. *Angew.*

Chem. Int. Ed. **2014**, *53*, 7122–7123; f) Horn, E. J.; Rosen, B. R.; Chen, Y.; Tang, J.; Chen, K.; Eastgate, M. D.; Baran, P. S. *Nature* **2016**, *533*, 77–81; g) Kawamata, Y.; Yan, M.; Liu, Z.; Bao, D.-H.; Chen, J.; Starr, J. T.; Baran, P. S. *J. Am. Chem. Soc.* **2017**, *139*, 7448–7451; h) Waldvogel, S. R.; Selt, M. *Angew. Chem. Int. Ed.* **2016**, *55*, 12578–12580; i) Hammerich, O.; Speiser, B., Eds. *Organic electrochemistry*, 5th ed., revised and expanded.; CRC Press: Boca Raton, Fla., 2016; j) Zhao, H.-B.; Hou, Z.-W.; Liu, Z.-J.; Zhou, Z.-F.; Song, J.; Xu, H.-C. *Angew. Chem. Int. Ed.* **2017**, *56*, 587–590; k) Lips, S.; Wiebe, A.; Elsler, B.; Schollmeyer, D.; Dyballa, K. M.; Franke, R.; Waldvogel, S. R. *Angew. Chem. Int. Ed.* **2016**, *55*, 10872–10876; l) Wiebe, A.; Schollmeyer, D.; Dyballa, K. M.; Franke, R.; Waldvogel, S. R. *Angew. Chem. Int. Ed.* **2016**, *55*, 11801–11805; m) Schulz, L.; Enders, M.; Elsler, B.; Schollmeyer, D.; Dyballa, K. M.; Franke, R.; Waldvogel, S. R. *Angew. Chem. Int. Ed.* **2017**, *56*, 4877–4881; n) Gütz, C.; Selt, M.; Bänziger, M.; Bucher, C.; Römelt, C.; Hecken, N.; Gallou, F.; Galvão, T. R.; Waldvogel, S. R. *Chem. Eur. J.* **2015**, *21*, 13878–13882;

(14) a) Francke, R.; Cericola, D.; Kötz, R.; Weingarth, D.; Waldvogel, S. R. *Electrochim. Acta* **2012**, *62*, 372–380; b) Eberson, L.; Hartshorn, M. P.; Persson, O. *J. Chem. Soc., Perkin Trans. 2* **1995**, 1735–1744; c) Eberson, L.; Hartshorn, M. P.; Persson, O.; Radner, F. *Chem. Commun.* **1996**, 2105–2112; d) Elsler, B.; Wiebe, A.; Schollmeyer, D.; Dyballa, K. M.; Franke, R.; Waldvogel, S. R. *Chem. Eur. J.* **2015**, *21*, 12321–12325; e) Hollóczki, O.; Berkessel, A.; Mars, J.; Mezger, M.; Wiebe, A.; Waldvogel, S. R.; Kirchner, B. *ACS Catal.* **2017**, *7*, 1846–1852.

(15) a) Tasker, S. Z.; Standley, E. A.; Jamison, T. F. *Nature* **2014**, *509*, 299–309; b) Ackerman, L. K. G.; Lovell, M. M.; Weix, D. J. *Nature* **2015**, *524*, 454–457;

(16) So, C. M.; Kwong, F. Y. *Chem. Soc. Rev.* **2011**, *40*, 4963–4972.

(17) Baciocchi, E.; Møllendal, H.; Aksnes, D. W.; Brekke, T.; Maartmann-Moe, K.; Tønnesen, H. H.; Tokii, T. *Acta Chem. Scand.* **1990**, *44*, 645–652.

(18) Hunsen, M. *Synthesis* **2005**, 2487–2490.

(19) Seganish, W. M.; DeShong, P. *J. Org. Chem.* **2004**, *69*, 1137–1143.

(20) a) Naumov, P.; Topcu, Y.; Eckert-Maksic, M.; Glasovac, Z.; Pavosevic, F.; Kochunnoonny, M.; Hara, H. *J. Phys. Chem. A* **2011**, *115*, 7834–7848; b) Muchall, H. M.; Werstiuk, N. H.; Lessard, J. *J. Mol. Struct (THEOCHEM)* **1999**, *469*, 135–142;

(21) Di Grandi, M. J. *Org. Biomol. Chem.* **2014**, *12*, 5331–5345.

(22) Gütz, C.; Klöckner, B.; Waldvogel, S. R. *Org. Process Res. Dev.* **2016**, *20*, 26–32.

Authors are required to submit a graphic entry for the Table of Contents (TOC) that, in conjunction with the manuscript title, should give the reader a representative idea of one of the following: A key structure, reaction, equation, concept, or theorem, etc., that is discussed in the manuscript. Consult the journal's Instructions for Authors for TOC graphic specifications.